Interplay between Nonlinearity, Scan Speed, Damping, and Electronics in Frequency Modulation Atomic-Force Microscopy

Michel Gauthier,[1] Ruben Pérez,[2] Toyoko Arai,[3] Masahiko Tomitori,[3] and Masaru Tsukada[1]

[1]*Department of Physics, Graduate School of Science, University of Tokyo, Hongo 7-3-1, Bunkyo-ku, Tokyo 113-0033, Japan*
[2]*Departamento de Física Teórica de la Materia Condensada, Universidad Autónoma de Madrid, E-28049 Madrid, Spain*
[3]*School of Materials Science, Japan Advanced Institute of Science and Technology,*
1-1 Asahidai, Tatsunokuchi, Nomi-gun, Ishikawa 923-1292, Japan

Numerical simulations of the frequency modulation atomic force microscope, including the whole dynamical regulation by the electronics, show that the cantilever dynamics is conditionally stable and that there is a direct link between the frequency shift and the conservative tip-sample interaction. However, a soft coupling between the electronics and the nonlinearity of the interaction may significantly affect the damping. A resonance between the scan speed and the response time of the system can provide a simple explanation for the spatial shift and contrast inversion between topographical and damping images, and for the extreme sensitivity of the damping to a tip change.

The rapid advance in nanoscale physics has constantly triggered innovative refinement of tools for detecting novel atomic scale phenomena. Scanning tunneling microscopy (STM) [1] exploits the exponential distance decay of the tip-sample tunneling current, and its confinement to the foremost atoms of the tip can provide atomically resolved images of conducting surfaces. Atomic force microscopy (AFM) [2] was devised to extend these capabilities to more general surfaces but the tip-sample contact area is often too large to permit atomic resolution. To remedy the situation, the amplitude modulation (AM) technique [3] (also known as tapping mode), where the change in amplitude of a vibrating cantilever due to the interaction is used for imaging the sample, has been adapted for AFM. However, the nonlinearity of the tip-sample force can lead to a complicated dynamical behavior [4] because two stable oscillation states coexist in many situations of interest.

Frequency modulation (FM) AFM [5] (also called noncontact AFM) has achieved the long-standing goal of true atomic resolution with AFM in UHV [6,7], as well as the direct measurement of the covalent bonding between the tip apex and sample atoms [8]. In FM-AFM, the dynamical system is more complicated because the oscillation amplitude of the cantilever is kept constant and the separation is regulated by measuring the change in the resonance frequency of the cantilever caused by the interaction force. Because the cantilever motion is highly sinusoidal, the measured frequency shift can be related to the interaction using perturbation theory [9–11].

In FM-AFM, the amount of excitation necessary to keep the oscillation amplitude constant (damping signal) can also be used as an imaging signal [12–17], but its magnitude and characteristics have been more difficult to quantify and interpret than the frequency shift. In principle, the damping signal could unleash important information about the surface such as that related to the phonon

local density of states in complete analogy with STM [18,19], although preliminary studies indicate that its magnitude is small compared to those reported in experiments. A number of mechanisms such as adhesion hysteresis [10,20–22] or Joule dissipation have been proposed to account for the large damping measured in experiments but many qualitative effects remain outstanding. For example, a small shift or even a contrast inversion is often observed between topographical and damping images for constant frequency shift scan [14–17]. Based on existing theoretical evidences, both adhesion hysteresis [21] and stochastic dissipation [18] predict a (in phase) normal contrast because the dissipation is caused by interatomic interaction and is more sensitive to the separation than the frequency shift signal itself. Joule dissipation should be expected to be rather small on lossless dielectric and metallic surfaces.

In this Letter, we stress the importance of identifying effects that pertain to the operation of FM-AFM, and consequently those which do not. This clearly requires a nonperturbative approach to the dynamical problem including the whole FM-AFM system; as we shall see, many effects found here are beyond the reach of perturbation theory [9,10,23]. To accomplish this, we perform numerical simulations of FM-AFM which are depicted in Fig. 1. The output of the detector, assumed to follow infinitely closely the motion of the cantilever $x(t)$, is sent to the amplitude regulator, FM demodulator, and the multiplier.

The amplitude regulator contains two main components. The first one, an analog rms-to-dc [24] (a peak-to-peak detector can be used alternatively), measures the amplitude of the cantilever oscillation according to the past motion of the cantilever,

$$A_{av}(t) = \sqrt{\frac{2}{\tau} \int_0^t x^2(t') e^{(t'-t)/\tau} dt' + A^{0^2} e^{-(t/\tau)}}. \quad (1)$$
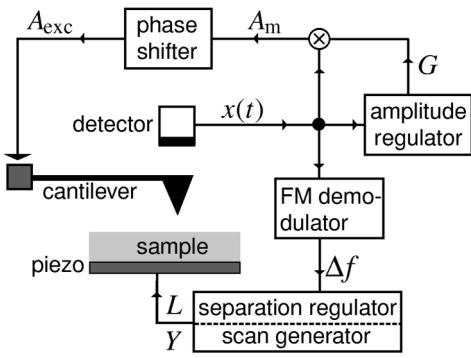
FIG. 1. The FM-AFM system. The cantilever motion $x(t)$ is first detected and then used to determine the gain G and, hence, the excitation signal A_{exc} needed to keep the amplitude constant, and the frequency shift Δf that regulates the separation L. The tip lateral position Y is regulated by the scan generator. The system is assumed to be noiseless.

The cantilever motion prior to the start of the numerical integration $t = 0$ is assumed to be perfectly sinusoidal with amplitude $A^0 = A_{set}$, the set amplitude of oscillation. The second module is a proportional integral (PI) controller [25]. It takes as input the average amplitude $A_{av}(t)$ and produces the gain G needed for constant amplitude operation:

$$G(t) = P[A_{av}(t) - A_{set}] + I \int_0^t [A_{av}(t') - A_{set}] dt' + G^0.$$
$$(2)$$

P and I are parameters set prior to the experiment, and G^0 is the gain factor consistent with A^0 prevailing before $t = 0$.

The equation governing the analog phase shifter is

$$A_{exc}(t) = A_m(t) - \frac{2}{\tau_{ps}} \int_0^t A_m(t') e^{(t'-t)/\tau_{ps}} dt' + \Delta A_{exc}^0,$$
$$(3)$$

where $A_m(t) = G(t)x(t)$ is the output of the multiplier, and $\Delta A_{exc}^0 \equiv [A_{exc}(0) - A_m(0)] e^{-(t/\tau_{ps})}$.

The FM demodulator is assumed to be a phase-locked loop (PLL). A PLL has three main components: a phase detector, a loop filter, and a voltage controlled oscillator (VCO). The PLL locks the VCO signal onto the cantilever motion so that the PLL output is essentially a dc signal proportional to the frequency shift and is described by the following two coupled nonlinear equations [26]:

$$u(t) = -\frac{2K}{\tau_{pll} A_{set}} \int_0^t dt' x(t') \sin[\Psi(t')] e^{(t'-t)/\tau_{pll}}, \quad (4)$$

$$\Psi(t) = \int_0^t [\omega_0 + u(t')] dt', \quad (5)$$

with ω_0 the intrinsic resonance frequency of the cantilever. u is the output of the (first-order) low-pass filter, $2K/A_{set}$ is the product of the gain constant of the phase detector and VCO. The frequency shift is then given by $\Delta f(t) = u(t)/2\pi$.

The separation regulator adjusts the tip-surface separation L so as to ensure that the output of the FM demodulator is kept close to the set frequency shift Δf_{set}:

$$L(t) = \frac{1}{\tau_L} \int_0^t \{P_L[\Delta f(t') - \Delta f_{set}] + L^O\} e^{(t'-t)/\tau_L} dt'. \quad (6)$$

The first-order low-pass filter mimics the response of the piezo and P_L is a quantity similar to P.

The equation of motion for the cantilever can thus be written as

$$\ddot{x} + \frac{\omega_0}{Q_0} \dot{x} + \omega_0^2 x = \frac{\omega_0^2}{k} F[x + L(t); Y(t)] + \omega_0^2 A_{exc}(t),$$
$$(7)$$

$Y(t) = \alpha \Theta(t - t_{scan})(t - t_{scan}) + Y_0$ being the lateral position of the tip which is regulated by the scan generator with $\Theta(t)$ the step function, and α the scan speed. k and Q_0 are the spring constant and intrinsic quality factor of the cantilever, respectively. $A_{exc}(t)$ and $L(t)$ are given by Eqs. (3) and (6), respectively. The numerical problem thus amounts to solving a set of integrodifferential equations. The constant step size fourth-order Runge-Kutta method is used for the numerical integration. Self-consistency is ensured at each substep for the PLL [Eqs. (4) and (5)]. In absence of tip crash, 400 steps per cycle is sufficient for proper integration.

Figure 2 shows the dynamics of the cantilever for a typical setup configuration. Initially, the tip is oscillating at a distance $L = 135$ Å and is then slowly brought to $L = 18.9$ Å from the surface. During the approach, the full electronics is on except for the separation regulator [$P_L = 0$ (open-loop), L^O is externally controlled (adjustable offset)] and the scan generator (no scanning). After the cantilever reaches some steady state, the separation regulator is slowly turned on (closed loop) and a new asymptotic behavior is established. The electronics linearizes most of the cantilever dynamics. First, the separation 2(a), frequency shift 2(b), and the average amplitude 2(c) are all well regulated. The frequency shift was confirmed to be insensitive to the details of the electronics and follow very closely that predicted by perturbation theory [9]. As shown in Fig. 2(d), the cantilever motion is very sinusoidal and its phase lag with respect to the (normalized) excitation signal A_{exc} is 90° (resonance). The small diminution (barely visible) of the gain ($\sim 0.013\%$) in Fig. 2(e) until $t \approx 2$ sec clearly indicates that anharmonic terms are negligible.

The increase of the damping of Fig. 2(e) is unexpected because the imprecision in the amplitude or phase [27] are negligible and the quality factor Q_0 is constant throughout the simulation. The extra energy is dissipated to the surface according to the perturbation formula $G = \frac{1}{Q_0} + \frac{\omega}{kA\pi} \int_0^{2\pi/\omega} F(x + L) \sin(\omega t) dt$ [10]. Because L is no longer *exactly* a constant, it provides a mechanism for which the force felt during the approach and retraction is different. When the separation regulator is fully operative (closed loop), the separation signal can be written as
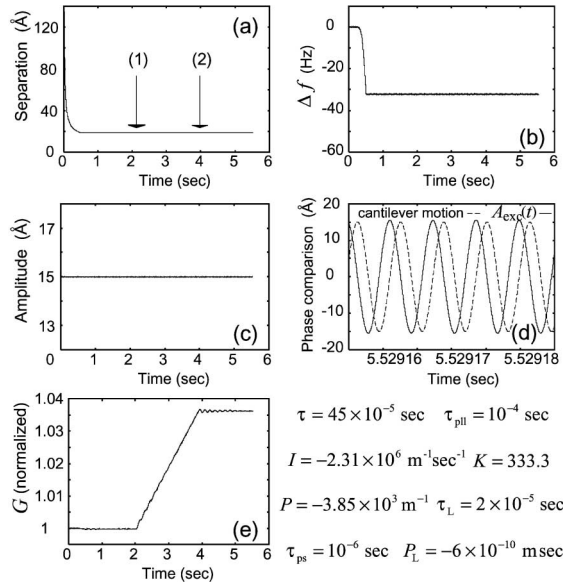
FIG. 2. The cantilever dynamics upon approach (no scanning). The separation (a), frequency shift (b), oscillation amplitude (c), cantilever motion (d), and gain (damping) (e) are shown. (1) and (2) in (a) indicate the time where the separation regulator is turned on and reaches full operation, respectively. The cantilever is characterized by $\omega_0 = 10^6\text{sec}^{-1}$, $k = 26\,\text{N/m}$, and $Q_0 = 24\,000$. The interaction potential is a Rydberg function with $b = 1.67\text{Å}^{-1}$, $R = 3\,\text{Å}$, and $U = 4 \times 10^{-11}\,\text{J}$. All parameters describing the electronics are also given.

$L(t) \approx L^O + L_1^C(t) + L_2^C$. $L_1^C(t)$ depends on the properties of the PLL and separation regulator [28] and L_2^C arises due to the weak coupling between the electronics and the tip-surface interaction and can be determined by solving the following implicit equations:

$$\Delta f^C = -\frac{f_0}{2kA\pi} \int_0^{2\pi} F(x + L)\cos\theta\,d\theta - \Delta f(L_{DC}), \quad (8)$$

$$L_2^C = P_L \Delta f^C. \quad (9)$$

Equation (8) is the perturbation formula [9] and Eq. (9) is obtained from Eq. (6). It can be seen that if the interaction force F is linear then $G \to 1/Q_0$ and there is no coupling among the electronic components, i.e., $L_2^C = 0$ and $\Delta f^C = 0$. In other words, the nonlinearity of the interaction plays an essential role for this dissipation mechanism to exist and could thus be made negligible by using extremely small amplitude [22]. The amplitude of the separation signal from $t \sim 4$ sec in Fig. 2(a) is about 0.03 Å (not visible on this scale). Note that the time scale of this mechanism matches that of the cantilever motion [28] and is thus effective at dissipating energy unless a precision better than ~ 0.01 Å for the separation is achieved.

Figure 3 shows topographical and damping profiles for two scan speeds. The model for the surface contains 112 atoms with a step. Before the scan, the tip is approached towards the surface as explained in Fig. 2. The scan speed affects dramatically the magnitude of the damping corrugation and its relative spatial phase. The contrast of the

damping signal is almost normal (50.47 Å/sec) or inverted (55.93 Å/sec) depending on the scan speed. The relative magnitude of the atomic corrugation of the damping signal is about ~1% which is directly comparable to some experiments where contrast inversion has been observed; for example, Refs. [15] (5%), [14] (less than 10%), and [16] (~2%). In contrast, the topographical profile is insensitive to the scan speed (even when $\alpha \sim 2500$ Å/sec) and follows closely the periodicity of the surface structure. For an ideal FM-AFM system, the frequency shift and oscillation amplitude would be exactly constant; here a corrugation smaller than 1 Hz and 0.1 Å is found, respectively.

The dependence of the damping signal corrugation and spatial shift on the scan speed is plotted in Figs. 4(a) and 4(b), respectively. The corrugation for the interaction F used in Figs. 2 and 3 (black line in Fig. 4) is clearly peaked around the velocity ~53 Å/sec for which the spatial shift is 2 Å (1/4 of the first layer spacing). When a long-range component (van der Waals) is added to the interaction (red), the corrugation increases but the spatial
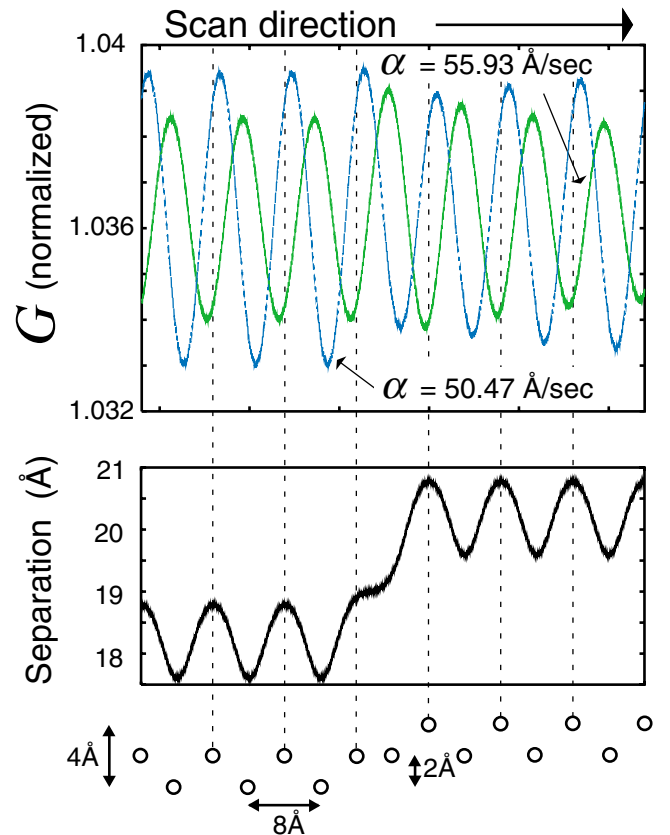

FIG. 3 (color). Damping and topographical profiles of a simple surface model with a step. Scanning is performed at constant frequency shift $\Delta f \approx -32.39$ Hz. The contrast is almost normal ($\alpha = 50.47$ Å/sec) or inverted ($\alpha = 55.93$ Å/sec) depending on the scan speed. The scan speed affects significantly the corrugation of the damping but not that of the separation. The orders of magnitude of the corrugation amplitude compare well with some experiments as discussed in the text.
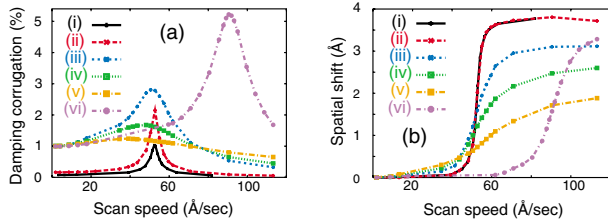
FIG. 4 (color). Effect of the scan speed on the atomic scale damping corrugation and spatial shift ($\Delta f \approx -32.39$ Hz). Six scenarios are shown: (i) F, (ii) $F - HR/[6(x+s)^2]$ with $H = 0.12365 \times 10^{-19}$ J, $R = 100$ Å, and $s = 4$ Å, F with a viscous dissipative process of the form $\gamma = \text{const} \sum (dF_i^\perp/dx)^2$ with (iii) $5P$, (iv) $10P$, (v) $20P$, and (vi) $5P$ and $3I$. F, P, and I are the interaction and the parameters of the PI controller, respectively, described in Fig. 2. The resonance implies that real dissipation to the surface is convoluted with the dynamical response of FM-AFM. The extreme sensitivity of the damping to a tip change could also be related to this resonance.

shift remains unchanged. Applying a large bias voltage as in Refs. [14,15] would therefore greatly enhance the damping corrugation, but here this is not related to Joule dissipation but to the change of the interaction itself. A resonance occurs when the time taken by the tip to cross two consecutive atoms in the uppermost sample layer matches the (transient) response time of the system. The latter was confirmed to depend on I (strongly) and P (weakly) of the PI controller [Eq. (2)]. Figure 4 shows what happens when a viscous dissipation process [18] exists for different values of I and P. In all cases, the resonance persists, although the peak height, position, and width are all related to the specific values of I and P. For very slow scan, the contrast is normal and the damping corrugation is independent of I and P. For faster scan, however, real dissipation is convoluted with the system operation; the change of the corrugation does not result from a change in the dissipation but is related to the way the amplitude is dynamically regulated. This unequivocally demonstrates the existence of an apparent dissipation mechanism in FM-AFM. It should be noted that increasing P directly deteriorates the precision of the damping signal, and the range of values of I for which the system remains stable is relatively narrow.

This resonance can also provide a simple explanation for the extreme sensitivity of the damping to a tip change [16,17]. A tip change directly affects the force which causes the damping corrugation to jump abruptly especially near the resonance.

A subtle remark about instabilities is now in order. In Ref. [23], it was pointed out that perturbation theory predicts the existence of *asymptotically* stable and unstable solutions. Here we found that all solutions near the resonance state are stable implying that the multi-valuedness of the solutions is very unlikely to play any role in FM-AFM as was previously suggested [29]. The feedback thus plays an *active* role even when a steady state has been reached. The stability is *conditional*, how-

ever, because the system response time is finite. In contrast to AM-AFM, an instability can lead only to a tip crash onto the surface. Abrupt changes in the interaction, dissipation, or excitation signal were numerically confirmed to be possible causes.

[1] G. Binnig and H. Rohrer, Helv. Phys. Acta **55**, 726 (1982).
[2] G. Binnig, C. Gerber, and C. Quate, Phys. Rev. Lett. **56**, 930 (1986).
[3] Y. Martin, C. C. Williams, and H. K. Wickramasinghe, J. Appl. Phys. **61**, 4723 (1987).
[4] R. Garcia and A. San Paulo, Phys. Rev. B **61**, R13381 (2000).
[5] T. R. Albrecht et al., J. Appl. Phys. **69**, 668 (1991).
[6] H. Ueyama et al., Appl. Phys. **34**, L1086 (1995).
[7] F. J. Giessibl, Science **267**, 68 (1995).
[8] M. A. Lantz et al., Science **291**, 2580 (2001).
[9] F. J. Giessibl, Phys. Rev. B **56**, 16 010 (1997).
[10] N. Sasaki and M. Tsukada, Jpn. J. Appl. Phys. **39**, L1334 (2000), Pt. 2.
[11] U. Dürig, New J. Phys. **2**, 5.1 (2000).
[12] U. Dürig, O. Züger, and A. Stalder, J. Appl. Phys. **72**, 1778 (1991).
[13] R. Lüthi et al., Surf. Rev. Lett. **4**, 1025 (1997).
[14] T. Arai and M. Tomitori, Appl. Phys. A **72**, S51 (2001); Appl. Surf. Sci. (to be published).
[15] M. Guggisberg et al., Surf. Sci. **461**, 255 (2000).
[16] C. Loppacher et al., Phys. Rev. B **62**, 13 674 (2000).
[17] R. Bennewitz et al., Phys. Rev. B **62**, 2074 (2000).
[18] M. Gauthier and M. Tsukada, Phys. Rev. B **60**, 11 716 (1999).
[19] L. N. Kantorovich, Phys. Rev. B **64**, 245409 (2001).
[20] U. Dürig, H. R. Steinauer, and N. Blanc, J. Appl. Phys. **82**, 3641 (1997).
[21] A. Abdurixit, A. Baratoff, and E. Meyer, Appl. Surf. Sci. **157**, 355 (2000).
[22] P. M. Hoffmann et al., Phys. Rev. Lett. **87**, 265502 (2001).
[23] M. Gauthier, N. Sasaki, and M. Tsukada, Phys. Rev. B **64**, 085409 (2001).
[24] Paul Horowitz and Winfield Hill, *The Art of Electronics* (Cambridge University Press, Cambridge, England, 1994).
[25] B. Gotsmann et al., Phys. Rev. B **60**, 11 051 (1999).
[26] R. E. Best, *Phase-Locked Loops Theory, Design, and Applications* (McGraw-Hill, New York, 1984).
[27] H. Hölscher et al., Phys. Rev. B **64**, 075402 (2001).
[28] $L_1^C(t) = (P_L/2\pi)\{[(\eta/\tau_L + 2\omega\beta)\sin(2\omega t) + (\beta/\tau_L - 2\omega\eta)\cos(2\omega t)]/[\tau_L(1/\tau_L^2 + 4\omega^2)(1/\tau^2 + 4\omega^2)]\} + \bar{L}_1^C$, where $\eta \equiv -K(\cos\epsilon/\tau + 2\omega\sin\epsilon)$, $\beta \equiv K(2\omega\cos\epsilon - \sin\epsilon/\tau)$, and $\Psi = \omega t + \epsilon$. $L_{DC} \equiv L^O + \bar{L}_1^C$, $\bar{L}_1^C = P_L[\Delta f(L_{DC}) - \Delta f_{set}]$, and $\Delta f(L_{DC}) = -K\sin\epsilon/(2\pi)$.
[29] M. Gauthier and M. Tsukada, Phys. Rev. Lett. **85**, 5348 (2000).